

**MFI zeolite-supported Ru nanoparticles for efficient conversion of pyroglutamic acid to 2-pyrrolidone**

Journal:	<i>Reaction Chemistry &amp; Engineering</i>
Manuscript ID	RE-ART-05-2021-000186.R1
Article Type:	Paper
Date Submitted by the Author:	12-Jul-2021
Complete List of Authors:	Otani, Akihiro; Tottori University Kuroda, Masaya; Tottori University, Center for Research on Green Sustainable Chemistry Suganuma, Satoshi; Tottori University, Center for Research on Green Sustainable Chemistry Tsuji, Etsushi; Tottori Daigaku, Department of Chemistry and Biotechnology, Graduate School of Engineering Katada, Naonobu; Tottori University, Department of Chemistry and Biotechnology, Graduate School of Engineering

# MFI zeolite-supported Ru nanoparticles for efficient conversion of pyroglutamic acid to 2-pyrrolidone

Akihiro Otani, Masaya Kuroda, Satoshi Suganuma,\* Etsushi Tsuji, Naonobu Katada

Center for Research on Green Sustainable Chemistry, Tottori University

4-101 Koyama-cho Minami, Tottori 680-8552, Japan

Phone: +81-857-31-5256; Fax: +81-857-31-5684; E-mail: suganuma@tottori-u.ac.jp

## Keywords

pyroglutamic acid; MFI zeolite; ruthenium; hydrogenation; decarbonylation

## Abstract

Pyroglutamic acid is readily formed through the dehydration-cyclization of glutamic acid, an abundant nonessential amino acid, by heating above 393 K without a catalyst. Herein, we describe the formation of 2-pyrrolidone by the hydrogenation and subsequent decarbonylation of pyroglutamic acid over MFI zeolite-supported Ru nanoparticles (Ru/MFI) under mild reaction conditions (433 K, 2 MPa H<sub>2</sub>). The yield of 2-pyrrolidone on Ru/MFI was influenced by the pH of the RuCl<sub>3</sub> aqueous solution used to impregnate Ru on the MFI zeolite. pH-adjustment led to strong adsorption of the cationic Ru precursors on the support and holding small and dispersed Ru nanoparticles on the MFI zeolite. The resulting catalyst provided a high yield of 2-pyrrolidone due to the high rate of decarbonylation into 2-pyrrolidone in the conversion of pyroglutamic acid. In addition, screening of various framework-type zeolites (commercially-available ones) as Ru catalyst supports demonstrated that MFI contains more cationic Ru (Ru<sup>δ+</sup>) than do the other zeolites tested, and Ru/MFI provided a higher yield of 2-pyrrolidone. The results suggest that Ru<sup>δ+</sup> loaded on MFI is workable as more active sites for the decarbonylation of the aldehyde intermediate

into 2-pyrrolidone compared to Ru<sup>0</sup> or other Ru species. This assumption was supported by comparison of the catalytic performance of Ru/MFI catalysts prepared by impregnation and ion exchange.

## 1. Introduction

Nitrogen-containing compounds such as amines, amides, and nitriles are utilized as raw materials for the synthesis of pharmaceuticals, polymers, organic semiconductors, and dyes. These raw materials are produced by inserting nitrogen into compounds of petrochemical origin. Ammonia is typically used as the nitrogen source, but industrial reactors for ammonia insertion require countermeasures to address toxicity and corrosion. In contrast, nitrogen-containing compounds obtained from biomass provide greener alternatives to petroleum and ammonia as sources of essential chemicals. Nowadays, studies on the conversion of organic nitrogen-containing compounds have been expanded<sup>1-5</sup>. It has been reported that shellfishery waste (chitin)<sup>6,7</sup> and proteins in microalgae reacted with CO<sub>2</sub><sup>8,9</sup> were utilized as the organic nitrogen-containing feedstocks, and oxygen-containing feedstocks derived from biomass were upgraded by ammonia insertion<sup>10,11</sup>. In addition, amino acids in proteins and peptides in biomass can be converted to nitrogen-containing intermediates and chemicals, lowering energy consumption compared to petroleum and ammonia processes<sup>12-15</sup>. Glutamic acid is the most abundant of the twenty common amino acids comprising proteins<sup>16</sup>. Bioethanol production from maize or wheat forms crude proteins in 20% dried distillers grains, and these crude proteins are soluble in water and contain 20% L-glutamic acid<sup>17-19</sup>. In addition, more than 3 million tons of L-glutamic acid is annually produced by the fermentation of sugar, and the production cost of L-glutamic acid is lower than that of other amino acids due to the high productivity of the production processes. L-glutamic acid is therefore the most abundant nitrogen-containing feedstock produced from plant biomass.

Pyroglutamic acid is obtained by heating glutamic acid above 393 K through dehydration-cyclization<sup>20</sup>. The conversion of pyroglutamic acid to chemical commodities was recently reported. For example, succinimide was formed by the decarboxylation and oxidation of pyroglutamic acid in the presence of AgNO<sub>3</sub> as a catalyst and S<sub>2</sub>O<sub>8</sub><sup>2-</sup> as an oxidant<sup>21</sup>. Hydrogenation of carboxyl groups in pyroglutamic acid provided pyroglutaminol, which in the co-presence of mineral acid was transformed to prolinol<sup>22</sup>. Decarboxylation of pyroglutamic acid formed 2-pyrrolidone on Pd/Al<sub>2</sub>O<sub>3</sub> in H<sub>3</sub>PO<sub>4</sub>-added aqueous solution at 523 K under a pressurized inert atmosphere<sup>23</sup>. Pd/Al<sub>2</sub>O<sub>3</sub> modified

by phosphoric acid also catalyzed the decarboxylation<sup>24</sup>. In contrast, we found that pyroglutamic acid was converted to 2-pyrrolidone on Ru/Al<sub>2</sub>O<sub>3</sub> in aqueous solution without an acid additive under a pressurized hydrogen atmosphere<sup>25</sup>. The Ru-loaded catalyst obviously exhibited higher yield of 2-pyrrolidone than the Pt-, Rh-, and Pd-loaded catalysts. The conversion of pyroglutamic acid to 2-pyrrolidone over Ru/Al<sub>2</sub>O<sub>3</sub> did not proceed in pressurized N<sub>2</sub> atmosphere, and therefore the decarboxylation of pyroglutamic acid did not proceed. The time courses in the conversion of pyroglutamic acid over Ru/Al<sub>2</sub>O<sub>3</sub> at pressurized H<sub>2</sub> atmosphere demonstrated the formation of pyroglutaminol as an intermediate at an initial time, and then pyroglutaminol was gradually converted to 2-pyrrolidone. The transformation of pyroglutaminol to 2-pyrrolidone via formation of 5-oxoprolinal was revealed by *in-situ* IR analysis. However, 5-oxoprolinal is reactive for decarbonylation into 2-pyrrolidone and has a short lifetime, making it impossible to detect in the analysis of the reaction solution. The evident reaction pathway (**Scheme 1**) involves hydrogenation of the carboxy group of pyroglutamic acid to an aldehyde group. The aldehyde product 5-oxoprolinal is converted to 2-pyrrolidone by decarbonylation, or hydrogenated to pyroglutaminol. Dehydrogenation of pyroglutaminol by a reversible reaction can also form 5-oxoprolinal and then 2-pyrrolidone.

2-Pyrrolidone is typically generated from petrochemical feedstock by inserting ammonia as a nitrogen source to manufacture  $\gamma$ -butyrolactone. 2-Pyrrolidone is a convenient solvent with a high boiling point and a high miscibility with water and most organic solvents. Biodegradable synthetic fibers are manufactured by the ring-opening polymerization of 2-pyrrolidone to produce nylon 4<sup>26</sup>. In *N*-vinyl-2-pyrrolidone, vinyl groups are connected to 2-pyrrolidone, and *N*-vinyl-2-pyrrolidone is used as a feedstock to manufacture polyvinylpyrrolidone, a useful solubilizer and dispersant<sup>27</sup>. 2-Pyrrolidone derivatives can also be used as pharmaceutical feedstocks. Alternative bio-based processes for the production of 2-pyrrolidone would therefore be important for obtaining a sustainable supply of chemical feedstocks.

The support material for metal-loaded catalysts influences catalytic performance, especially activity and product selectivity. The properties of the active species depend on the interaction between the metal and the support, and these properties alter the electronic and dispersed states of metals. Many oxide supports bear surface hydroxy groups, and the adsorbability of metal precursors on the surface OH groups is influenced by the pH of the solution used for catalyst preparation. In this paper, we report that MFI zeolite-supported Ru-catalyst exhibits high catalytic

performance in the conversion of pyroglutamic acid to 2-pyrrolidone. The properties of the active Ru species are influenced by the pH of the precursor solution used to impregnate the support with Ru. We show that  $\text{Ru}^{\delta+}$  on MFI zeolite is a highly active species for the efficient formation of 2-pyrrolidone by comparing Ru ion-exchange with impregnation for catalyst preparation.

## 2. Experimental

### 2.1 Catalyst preparation

All reagents were used as obtained without further treatment. Loaded 5 wt.% Ru catalysts were typically prepared by impregnation on  $\text{Al}_2\text{O}_3$  (JRC-ALO-6, Catalysis Society of Japan),  $\text{ZrO}_2$  (JRC-ZRO-6, Catalysis Society of Japan),  $\text{TiO}_2$  (JRC-TIO-9, Catalysis Society of Japan), MgO (Fujifilm Wako Pure Chemical Corporation),  $\text{CeO}_2$  (JRC-CEO-2, Catalysis Society of Japan),  $\text{Nb}_2\text{O}_5$  (JRC-NBO-1, Catalysis Society of Japan),  $\text{SiO}_2$  (JRC-SIO-13, Catalysis Society of Japan), and commercial zeolites with various frameworks of MFI (Na-form,  $\text{Si}/\text{Al}_2 = 90$ , JRC-Z5-90NA(1), Catalysis Society of Japan), FAU (Na-form,  $\text{Si}/\text{Al}_2 = 5.3$ , JRC-ZY-5.3NA, Catalysis Society of Japan), MOR (H-form,  $\text{Si}/\text{Al}_2 = 90$ , JRC-Z-HM90(1), Catalysis Society of Japan), and \*BEA (H-form,  $\text{Si}/\text{Al}_2 = 150$ , JRC-Z-HB150(1), Catalysis Society of Japan). In a typical impregnation procedure, the solid support was stirred in  $\text{RuCl}_3$  aqueous solution for 1 h, followed by evaporating the water at 343 K and drying at 383 K overnight. The solid powder was reduced using  $\text{H}_2$  at 573 K for 3 h to obtain the final products. To conduct impregnation in a pH-adjusted aqueous solution, the pH of the solution was raised from 1.8 to 2.8–8.9 using  $\text{NH}_4\text{OH}$  solution; subsequent steps are the same as in the typical procedure. Ru/MFI was also prepared by the ion-exchange of Ru. MFI zeolite (2 g) was added to  $\text{RuCl}_3$  aqueous solution (100 mL, Ru content  $1 \text{ g L}^{-1}$ ) after adjusting to pH 3, and the mixture was stirred at room temperature overnight. The as-formed catalyst was filtered and dried at 383 K overnight, and then the solid powder was reduced with  $\text{H}_2$  at 573 K for 3 h to obtain the final product.

### 2.2 Catalyst characterization

The crystalline phases of the catalysts were analyzed by X-ray diffraction (XRD, Rigaku Ultima IV diffractometer) with  $\text{CuK}_\alpha$  radiation in the  $2\theta$  range from 10 to  $80^\circ$ . Transmission electron microscopy (TEM, JEOL

JEM1400 Plus) was conducted at an acceleration voltage of 80.0 kV. Samples were dispersed on copper grids using ethanol after ultrasonic pretreatment. The amounts of CO chemisorbed on the catalysts were recorded at 323 K from 0.01 to 50 kPa by using a volumetric adsorption apparatus (MicrotracBEL BELSORP-max). Prior to gas adsorption, the samples were heated at 573 K in O<sub>2</sub> flow, and then H<sub>2</sub> flow, and evacuated with cooling to 323 K. Infrared (IR) analysis of CO chemisorbed on the catalysts was performed by using an IR spectrometer (FT/IR-4200, JASCO). The catalyst powder was compressed at 20 MPa into a self-supporting disk 1 cm in diameter and then set in the in situ IR cell (MicrotracBEL IRMS-TPD). Prior to gas adsorption, the sample was heated at 573 K in a H<sub>2</sub>(5%)/Ar flow (50 mL min<sup>-1</sup>) and then cooled to 298 K in an Ar flow (50 mL min<sup>-1</sup>). After recording an IR reference spectrum, the IR cell was evacuated, charged with CO at 5 kPa, and evacuated again. An IR spectrum of adsorbed CO on the catalyst was measured in an Ar flow (50 mL min<sup>-1</sup>). The difference spectrum was calculated by subtracting the IR reference spectrum. The Ru content in the catalyst was measured using inductively coupled plasma optical emission spectroscopy (ICP-OES, Agilent 5110).

### 2.3 Catalytic testing

The catalytic activity for the conversion of L-pyroglutamic acid (Tokyo Chemical Industry) was measured using the reactant as received. In a typical run, an aqueous solution of pyroglutamic acid (0.026 mol L<sup>-1</sup>, 50 mL) and a catalyst (0.2 g) was charged into a batch autoclave reactor (120 mL, Taiatsu Techno). After sealing, the interior atmosphere was purged and pressurized using H<sub>2</sub> (2 MPa). The solution was stirred at 500 rpm and heated at 433 K. After the reaction, the autoclave was cooled to room temperature. The catalyst was separated from the solution by centrifugation. The resulting supernatant was mixed with tetraethylene glycol dimethyl ether (Tokyo Chemical Industry) as an internal standard and analyzed using gas chromatograph (GC-2014, Shimadzu) with a capillary column (HP-INNOWax) and a flame ionization detector (FID).

Conversion was calculated using the following expression: ([Conversion (%)] = (1 - [detected reactant (mol)] / [charged reactant (mol)]) × 100).

The product yield was calculated using the following expression: ([Yield (%)] = [detected product (mol)] / [charged reactant (mol)]) × 100)

Others indicated undetected products by GC and their yield were calculated from the expression: ([conversion (%)] – [total yield of detected products (%)]).

The amount of leached Ru species was analyzed by inductivity coupled plasma optical emission spectrometer (Agilent, 5110ICP-OES). The reaction solution was filtered by a syringe filter with 0.2  $\mu\text{m}$  of pore diameter before the analysis because ICP-OES may break down due to the solution containing a large amount of coarse Ru particles. The wavelength of 240.272 nm was selected for Ru detection.

### 3. Results

#### 3.1 Support screening of Ru-loaded catalyst for pyroglutamic acid conversion

Supports for Ru-loaded catalysts were screened for the conversion of pyroglutamic acid to 2-pyrrolidone (**Figure 1**). The catalysts were prepared in  $\text{RuCl}_3$  solution at pH 1.8 (pH not adjusted).  $\text{Al}_2\text{O}_3$  was previously used for the conversion of glutamic acid<sup>25</sup> and provided a high yield of 2-pyrrolidone, similar to the present study. Amphoteric oxides ( $\text{ZrO}_2$  and  $\text{TiO}_2$ ) similar to  $\text{Al}_2\text{O}_3$  and an acidic oxide ( $\text{Nb}_2\text{O}_5$ ) formed more pyroglutaminol than 2-pyrrolidone, while basic oxides ( $\text{MgO}$  and  $\text{CeO}_2$ ) formed much less hydrogenation product than the other supports. MFI zeolite provided the highest 2-pyrrolidone yield among the supports tested and is effective for the formation of 2-pyrrolidone. However, Ru leached out from the support and the recovered solution was slightly black.

#### 3.2 Influence of pH of Ru impregnation solution on catalyst performance of Ru/MFI

Leaching was controlled by impregnating MFI zeolite in a pH-adjusted  $\text{RuCl}_3$  solution during catalyst preparation. The pH of the initial  $\text{RuCl}_3$  solution was 1.8, which could be lower than the isoelectric point of MFI zeolite. The pH was therefore raised by adding  $\text{NH}_4\text{OH}$  solution, and the amount of adsorbed Ru cations on the MFI support was increased. **Figure S1** shows XRD patterns for the prepared catalysts. Diffraction peaks associated with MFI zeolite were apparent for all samples, indicating that the crystal structure of MFI zeolite was retained throughout the preparation procedure. Small peaks at 38 – 44° observed for all catalysts indicate hexagonal ruthenium. TEM images and particle size distributions are shown in **Figure S2**. The impregnated Ru catalysts at pH 1.8 and 2.8 had narrow particle size distributions and increasing the pH broadened the distribution. The average particle diameters

determined from the TEM images are shown in **Table 1**. Increasing the pH of the preparation increased the Ru particle size up to pH 6.0, but the particle size then decreased at pH 8.9. The amount of chemisorbed CO on Ru (CO/Ru ratio) was calculated on the basis of CO chemisorption results at 323 K. The CO/Ru ratios are shown in **Table 1**. The Co/Ru ratios for the impregnated Ru catalysts at pH 1.8 and 2.8 were higher than those for the other catalysts, indicating the presence of small dispersed Ru particles, consistent with the TEM results.

The effect of the pH of the Ru impregnation solution on the performance of Ru-loaded catalysts on MFI zeolite was investigated in the conversion of pyroglutamic acid (**Figure 2**). Impregnated catalysts at pH 1.8 and 2.8 provided higher yields of 2-pyrrolidone than the other catalysts. The reaction solution over the impregnated catalyst at pH 2.8 was not entirely black. The Ru amount in the reaction solution over the impregnated catalysts at pH 1.8 and 2.8 were 0.28 and 0.20 ppm, and the leached amount of Ru from the catalysts were 0.13 and 0.09 mol%, respectively. Increasing the pH of the original RuCl<sub>3</sub> solution (pH 1.8) restricted Ru leaching from the MFI support and the reaction solution did not turn black by the formation of black Ru particles (particle size: > 0.2 μm) and Ru dissolving in the reaction solution. However, a pH >2.8 decreased 2-pyrrolidone yield while increasing pyroglutaminol yield. Therefore, a Ru impregnation solution with a pH of 2.8 favors the efficient production of 2-pyrrolidone from pyroglutamic acid and increases catalyst stability.

### 3.3 Impregnation of Ru on zeolite support under fixed pH conditions

The zeolite framework affects ionic strength and porosity, which influence the function of the zeolite as a catalyst support. Accordingly, zeolites with different frameworks ((MFI, FAU, MOR, and \*BEA)-supported Ru catalysts) were prepared through impregnation using pH 2.8 solutions. SiO<sub>2</sub> and Al<sub>2</sub>O<sub>3</sub> were also used as supports for comparison. **Figure S3** shows TEM images and particle size distributions for the Ru catalysts. Al<sub>2</sub>O<sub>3</sub>, FAU, and \*BEA had similar Ru particle size distributions to MFI, while wider distributions were observed for MOR and SiO<sub>2</sub>. The average particle diameters of Al<sub>2</sub>O<sub>3</sub>, FAU, \*BEA, and MFI were 2.8–3.5 nm, and Ru particles were uniformly dispersed on the supports (**Table 2**). Some Ru particles aggregated on MOR and SiO<sub>2</sub>, and their average diameters were larger than that for the other catalysts. The CO/Ru ratios are shown in **Table 2** and follow the order Al<sub>2</sub>O<sub>3</sub> > MFI > FAU ≈ \*BEA > MOR > SiO<sub>2</sub>.

IR measurements of adsorbed CO on the catalysts were used to identify the Ru oxidation states (**Figure 3**). CO was adsorbed on the catalysts without atmospheric exposure after hydrogen reduction at 573 K as a pretreatment. Two main bands, observed at 2020 and 2080  $\text{cm}^{-1}$ , were previously assigned to CO linearly adsorbed on metallic  $\text{Ru}^0$  ( $\text{Ru}^0\text{-CO}$ ) and CO molecules adsorbed on cationic  $\text{Ru}^{\delta+}$  ( $\text{Ru}^{\delta+}\text{-CO}$ ), respectively<sup>28,29</sup>. A shoulder at around 2000  $\text{cm}^{-1}$  was also present and was due to CO adsorbed on isolated  $\text{Ru}^0$  atoms<sup>28,29</sup>. Moreover, two small bands were observed at 2135 and 2165  $\text{cm}^{-1}$  and were due to multiple CO molecules adsorbed on cationic ruthenium as  $\text{Ru}^{\delta+}\text{-(CO)}_3$  and  $\text{Ru}^{2+}\text{-(CO)}_n$ , respectively<sup>30,31</sup>. The latter species was formed as a result of ionic exchange with zeolite cations. The bands related to CO were essentially absent on  $\text{Ru/SiO}_2$ . The presence of  $\text{Ru}^0\text{-CO}$ ,  $\text{Ru}^{\delta+}\text{-CO}$ , and  $\text{Ru}^{\delta+}\text{-(CO)}_3$  on all the zeolites and  $\text{Al}_2\text{O}_3$  suggested the presence of ruthenium metals and oxidized ruthenium. The absorbance for  $\text{Ru}^{\delta+}\text{-CO}$  was the same as that for  $\text{Ru}^0\text{-CO}$  on  $\text{Al}_2\text{O}_3$ , FAU, MOR, and \*BEA, while the proportion of the absorbance for  $\text{Ru}^{\delta+}\text{-CO}$  to  $\text{Ru}^0\text{-CO}$  was about 2 on MFI. Therefore, MFI contained more cationic ruthenium than the other catalysts.

**Figure 4** shows the conversion of pyroglutamic acid over the prepared Ru catalysts.  $\text{SiO}_2$  formed more pyroglutaminol than 2-pyrrolidone, while  $\text{Al}_2\text{O}_3$  provided a high yield of 2-pyrrolidone due to the presence of many active sites, as evident from the greater amount of chemisorbed CO. FAU, MOR, and \*BEA had lower amounts of chemisorbed CO, and thus provided a lower yield of 2-pyrrolidone than did  $\text{Al}_2\text{O}_3$ . However, the yield of 2-pyrrolidone on MFI was higher than that on  $\text{Al}_2\text{O}_3$ , indicating that cationic ruthenium on MFI could form more 2-pyrrolidone than ruthenium metal, despite the smaller amount of chemisorbed CO than on  $\text{Al}_2\text{O}_3$ .

#### 3.4 Loading Ru on zeolites by ion-exchange

Cationic ruthenium loaded on zeolite was presumed to be formed on ion-exchange sites (i.e., Brønsted acid sites) of the original MFI zeolite. Accordingly, ion-exchange Ru loading on MFI zeolite might provide higher cationic ruthenium loading than Ru impregnation. In this study, ruthenium was loaded on MFI zeolite through ion exchange (Ru/MFI-ie). The previously described catalysts contained 5 wt.% Ru, whereas the Ru content of Ru/MFI-ie was 2.1 wt.% (**Table 3**). To compare the catalytic activity and physical properties achieved by ion exchange and impregnation (Ru/MFI-imp), Ru/MFI-imp was prepared by impregnation with a similar loading as Ru/MFI-ie. Ru/ $\text{Al}_2\text{O}_3$ -imp was

also prepared through impregnation as a control. **Figure S4** shows TEM images and particle size distributions for ruthenium. The Ru particles on Ru/MFI-ie were smaller than those on Ru/MFI-imp and Ru/Al<sub>2</sub>O<sub>3</sub>-imp. As shown in **Table 3**, the CO/Ru ratio on MFI was slightly increased by ion exchange compared with impregnation but the ratio on Ru/Al<sub>2</sub>O<sub>3</sub>-imp was higher than that on the Ru/MFI catalysts.

**Figure 5** shows IR spectra of adsorbed CO on the catalysts. The main band at 2020 cm<sup>-1</sup> for Ru/Al<sub>2</sub>O<sub>3</sub>-imp and Ru/MFI-imp was assigned to CO linearly adsorbed on Ru<sup>0</sup> (Ru<sup>0</sup>-CO), and the bands at 2080 and 2135 cm<sup>-1</sup> were attributed to Ru<sup>δ+</sup>-CO and Ru<sup>δ+</sup>-(CO)<sub>3</sub>, respectively. Additionally, Ru/MFI-imp showed bands at 1895 and 2170 cm<sup>-1</sup> that were assigned to bridge-type CO adsorbed on Ru (Ru<sub>2</sub>-(CO)) and multiple CO molecules adsorbed on cationic ruthenium (Ru<sup>2+</sup>-(CO)<sub>n</sub>), respectively<sup>30-32</sup>. The main band of Ru/MFI-ie was ascribed to Ru<sup>δ+</sup>-CO and the smaller bands to Ru<sup>0</sup>-CO, Ru<sup>δ+</sup>-(CO)<sub>3</sub>, and Ru<sup>2+</sup>-(CO)<sub>n</sub>. These results suggested that Ru/MFI-ie contained more Ru<sup>δ+</sup> as the main species than Ru/MFI-imp and Ru/Al<sub>2</sub>O<sub>3</sub>-imp.

The effect of Ru loading by ion exchange on the conversion of pyroglutamic acid was investigated by comparison with Ru/Al<sub>2</sub>O<sub>3</sub>-imp and Ru/MFI-imp (**Figure 6**). Ru/MFI-ie provided a higher yield of 2-pyrrolidone than catalysts prepared by Ru impregnation. The total yield of 2-pyrrolidone and pyroglutaminol obtained using Ru/MFI-ie was 81%, together with small amounts of byproducts containing pyrrolidine and 5-methyl-2-pyrrolidone, whereas the yield of these byproducts using Ru/Al<sub>2</sub>O<sub>3</sub>-imp was 50%. These findings suggested that the amount of Ru<sup>δ+</sup> increased with increasing yield of 2-pyrrolidone and restrained side reactions.

#### 4. Discussion

The oxide supports for Ru-loaded catalysts influence catalytic activity in the conversion of pyroglutamic acid to 2-pyrrolidone (**Figure 1**). Al<sub>2</sub>O<sub>3</sub> and MFI zeolite exhibited higher yields of 2-pyrrolidone in comparison to other products. MFI zeolite provided superior activity but a small amount of Ru leached from the MFI support. The black suspended solids could be removed after the reaction by passing the reaction mix through a syringe filter, indicating that the Ru leached as coarse aggregates, possibly due to weak interaction between the support and Ru aggregates. During catalyst preparation, MFI zeolite was initially impregnated with Ru using a pH 1.8 RuCl<sub>3</sub> solution. The Ru species in this solution were [RuCl<sub>4</sub>(H<sub>2</sub>O)<sub>2</sub>]<sup>-</sup> and [RuCl<sub>3</sub>(H<sub>2</sub>O)<sub>3</sub>] and these species were difficult to adsorb on

the surface of MFI zeolite, causing them to aggregate<sup>33</sup>. The formed Ru aggregates leached from the catalyst during the conversion of pyroglutamic acid. However, increasing the pH changed the Ru precursors to  $[\text{RuCl}_2(\text{H}_2\text{O})_4]^+$ ,  $[\text{RuCl}(\text{H}_2\text{O})_5]^{2+}$ , and polymeric species.  $[\text{RuCl}_2(\text{H}_2\text{O})_4]^+$  and  $[\text{RuCl}(\text{H}_2\text{O})_5]^{2+}$  can be strongly adsorbed and be widely dispersed on the surface of MFI zeolite.

The pH of the  $\text{RuCl}_3$  solution was raised from 1.8 by the addition of  $\text{NH}_4\text{OH}$  solution to 2.8, 3.7, 6.0, and 8.9. Ru/MFI catalysts impregnated in solution at pH 2.8 had smaller and more dispersed Ru particles than the catalysts impregnated at the other pH values (**Table 1**) due to strong adsorption of the cationic Ru precursors on the MFI support. The Ru/MFI catalyst high yield of 2-pyrrolidone and minimal Ru leaching in the conversion of pyroglutamic acid (**Figure 2**). In contrast,  $\text{RuCl}_3$  solutions at  $\text{pH} > 2.8$  formed polymeric Ru species<sup>33</sup> and the impregnated catalysts in the solution had Ru particles  $> 5$  nm in diameter. High pH decreased the 2-pyrrolidone yield and increased the pyroglutaminol yield, indicating that Ru grain coarsening lowers the rate of 5-oxoprolinal decarbonylation (**Scheme 1**).

Ruthenium was impregnated onto various framework-type zeolites,  $\text{SiO}_2$ , and  $\text{Al}_2\text{O}_3$  using pH 2.8  $\text{RuCl}_3$  solution. The Ru particle sizes on  $\text{Al}_2\text{O}_3$ , FAU, and \*BEA were similar to that on MFI, while wider particle size distributions were observed for  $\text{SiO}_2$  and MOR due to formation of Ru aggregates (**Table 2**). MFI showed a higher CO/Ru ratio (amount of chemisorbed CO on Ru) than the other zeolites and  $\text{SiO}_2$ , but lower than that for  $\text{Al}_2\text{O}_3$ . IR measurements of adsorbed CO on the catalysts suggested the presence of  $\text{Ru}^0$  and  $\text{Ru}^{\delta+}$  on all the catalysts, excluding  $\text{SiO}_2$  (**Figure 3**). MFI contained more cationic ruthenium ( $\text{Ru}^{\delta+}$ ) than the other catalysts. XPS (X-ray photoelectron spectroscopy) analysis is impossible to detect photoelectrons from  $\text{Ru}^{\delta+}$  on the ion-exchangeable sites in the micropore due to mean free path smaller than several nm of photoelectrons in the solid, but the existence of  $\text{Ru}^{\delta+}$  on Ru/MFI was revealed in the previous reports<sup>34,35</sup>. Ion-exchangeable sites on MFI zeolite generate strong Brønsted acid sites by the addition of protons<sup>36</sup>. This means that the ion-exchangeable sites hold strong electron affinity, and therefore  $\text{Ru}^{\delta+}$  can be stabilized on the surface. In the conversion of pyroglutamic acid, Ru/MFI exhibited higher yield of 2-pyrrolidone than did Ru/ $\text{Al}_2\text{O}_3$  (**Figure 4**), despite the smaller amount of chemisorbed CO (CO/Ru ratio) and thus fewer active sites. The other zeolite-supported Ru catalysts had fewer active sites and a lower  $\text{Ru}^{\delta+}$  content than did Ru/MFI, and thus showed low yields of 2-pyrrolidone and high yields of pyroglutaminol. These results show

that  $\text{Ru}^{\delta+}$  loaded on MFI provided more active sites for the decarbonylation of 5-oxoprolinal to 2-pyrrolidone than  $\text{Ru}^0$  and other Ru species.

Ru loading by ion-exchange on MFI presumably provided many  $\text{Ru}^{\delta+}$  species. Ru/MFI-ie prepared by ion-exchange had almost the same Ru particle size and CO/Ru ratio as Ru/MFI-imp and Ru/ $\text{Al}_2\text{O}_3$ -imp prepared by impregnation (**Table 3**). IR measurements of adsorbed CO on the catalysts suggested that Ru/MFI-ie contained more  $\text{Ru}^{\delta+}$  species than did Ru/MFI-imp and Ru/ $\text{Al}_2\text{O}_3$ -imp (**Figure 5**). Ru/MFI-ie showed higher yield of 2-pyrrolidone than did Ru/MFI-imp and Ru/ $\text{Al}_2\text{O}_3$ -imp. These results substantiate the assumption that  $\text{Ru}^{\delta+}$  loaded on MFI provided more active sites for the decarbonylation of 5-oxoprolinal to 2-pyrrolidone than the other Ru species.

## 5. Conclusions

The conversion of pyroglutamic acid to 2-pyrrolidone was highly catalyzed by MFI zeolite-supported ruthenium nanoparticles (Ru/MFI). The Ru particle size and catalytic performance of Ru/MFI were influenced by adjusting the pH of the  $\text{RuCl}_3$  solution for Ru impregnation of the MFI zeolite. The impregnated catalyst at pH 2.8 had smaller and more dispersed Ru particles than did catalysts prepared at other pH values due to strong adsorption of the cationic Ru precursors on MFI zeolite. The Ru/MFI catalyst exhibited high yield of 2-pyrrolidone and restricted Ru leaching during the reaction. Higher pH values for the precursor solution led to Ru grain coarsening on the MFI zeolite, resulting in lower yields of 2-pyrrolidone. In addition, screening of commercial framework-type zeolites as Ru catalyst supports revealed that Ru/MFI contained more cationic ruthenium ( $\text{Ru}^{\delta+}$ ) than  $\text{Ru}^0$  and other Ru species, while other zeolite-supported Ru catalysts had a minor  $\text{Ru}^{\delta+}$  content. These results indicate that the ion-exchangeable sites with strong electron affinity on MFI zeolite stabilize  $\text{Ru}^{\delta+}$  compared with ion-exchangeable sites on other zeolites. Ru/MFI exhibited high yield of 2-pyrrolidone while the other zeolite-supported catalysts showed high yield of pyroglutaminol. This finding suggests that  $\text{Ru}^{\delta+}$  on MFI zeolite provides more active sites for the decarbonylation of 5-oxoprolinal, the aldehyde generated by the hydrogenation of pyroglutamic acid, to 2-pyrrolidone compared to  $\text{Ru}^0$  and other Ru species. Comparison of the catalytic performance of Ru/MFI catalysts prepared by impregnation and ion-exchange showed that the catalyst prepared by ion-exchange bound more  $\text{Ru}^{\delta+}$  and showed a higher yield of 2-pyrrolidone. These results substantiate the assumption that  $\text{Ru}^{\delta+}$  loaded on MFI provide more active sites for the

decarbonylation of 5-oxoproline to 2-pyrrolidone compared to other Ru species.

## Conflicts of interest

There are no conflicts to declare.

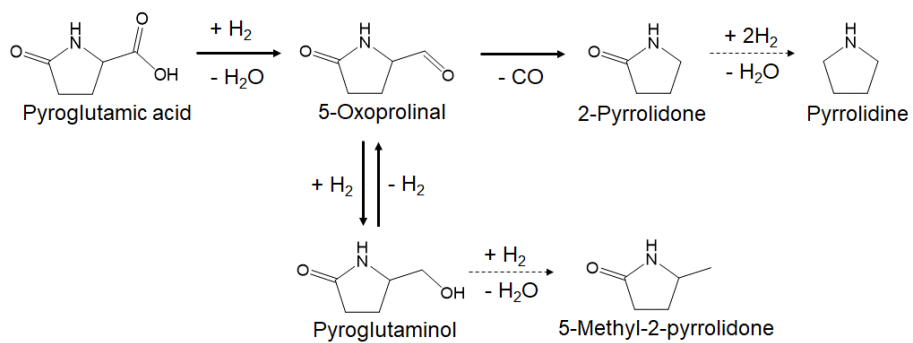
## Acknowledgements

A part of this work was supported by JST CREST Grant Number JPMJCR17P1, Japan and JSPS KAKENHI Grant Number 18K14261 and 21H01717.

## References

- 1 S. E. Davis, M. S. Ide and R. J. Davis, *Green Chem.*, 2013, **15**, 17–45.
- 2 M. J. Gilkey and B. Xu, *ACS Catal.*, 2016, **6**, 1420–1436.
- 3 H. Kobayashi and A. Fukuoka, *Green Chem.*, 2013, **15**, 1740–1763.
- 4 M. Besson, P. Gallezot and C. Pinel, *Chem. Rev.*, 2014, **114**, 1827–1870.
- 5 X. Li, P. Jia and T. Wang, *ACS Catal.*, 2016, **6**, 7621–7640.
- 6 X. Chen, S. Song, H. Li, G. Gözaydın and N. Yan, *Acc. Chem. Res.*, 2021, **54**, 1711–1722.
- 7 X. Gao, X. Chen, J. Zhang, W. Guo, F. Jin and N. Yan, *ACS Sustain. Chem. Eng.*, 2016, **4**, 3912–3920.
- 8 Y. Yang, H. Zhong, R. He, X. Wang, J. Cheng, G. Yao and F. Jin, *Green Chem.*, 2019, **21**, 1247–1252.
- 9 J. Li, P. Zhu, H. Zhong, Y. Yang, J. Cheng, Y. Wang and F. Jin, *ACS Sustain. Chem. Eng.*, 2021, **9**, 4791–4800.
- 10 Y. Wang, S. Furukawa, X. Fu and N. Yan, *ACS Catal.*, 2020, **10**, 311–335.
- 11 S. Song, V. Fung Kin Yuen, L. Di, Q. Sun, K. Zhou and N. Yan, *Angew. Chemie - Int. Ed.*, 2020, **59**, 19846–19850.
- 12 J. Sanders, E. Scott, R. Weusthuis and H. Mooibroek, *Macromol. Biosci.*, 2007, **7**, 105–117.
- 13 E. Scott, F. Peter and J. Sanders, *Appl. Microbiol. Biotechnol.*, 2007, **75**, 751–762.
- 14 L. Claes, R. Matthessen, I. Rombouts, I. Stassen, T. DeBaerdemaeker, D. Depla, J. A. Delcour, B. Lagrain and D. E. De Vos, *ChemSusChem*, 2015, **8**, 345–352.
- 15 M. Tamura, R. Tamura, Y. Takeda, Y. Nakagawa and K. Tomishige, *Chem. - A Eur. J.*, 2015, **21**, 3097–3107.
- 16 T. M. Lammens, M. C. R. Franssen, E. L. Scott and J. P. M. Sanders, *Biomass and Bioenergy*, 2012, **44**, 168–181.
- 17 Y. Kim, N. S. Mosier, R. Hendrickson, T. Ezeji, H. Blaschek, B. Dien, M. Cotta, B. Dale and M. R. Ladisch, *Bioresour. Technol.*, 2008, **99**, 5165–5176.
- 18 R. L. Belyea, K. D. Rausch and M. E. Tumbleson, *Bioresour. Technol.*, 2004, **94**, 293–298.
- 19 M. J. Spieths, M. H. Whitney and G. C. Shurson, *J. Anim. Sci.*, 2002, **80**, 2639.
- 20 Y. Teng, E. L. Scott and J. P. M. Sanders, *J. Chem. Technol. Biotechnol.*, 2012, **87**, 1458–1465.

- 
- 21 J. Deng, Q. G. Zhang, T. Pan, Q. Xu, Q. X. Guo and Y. Fu, *RSC Adv.*, 2014, **4**, 27541–27544.
- 22 J. E. Holladay, T. A. Werpy and D. S. Muzatko, *Appl. Biochem. Biotechnol.*, 2004, **115**, 0857–0870.
- 23 F. De Schouwer, L. Claes, N. Claes, S. Bals, J. Degrève and D. E. De Vos, *Green Chem.*, 2015, **17**, 2263–2270.
- 24 X. Shi, X. Ye, J. Cheng, X. Wang, P. Chen, Y. Yang and T. Wang, *ChemistrySelect*, 2021, **6**, 4124–4128.
- 25 S. Suganuma, A. Otani, S. Joka, H. Asako, R. Takagi, E. Tsuji and N. Katada, *ChemSusChem*, 2019, **12**, 1381–1389.
- 26 K. Hashimoto, T. Hamano and M. Okada, *J. Appl. Polym. Sci.*, 1994, **54**, 1579–1583.
- 27 E. Senogles and R. Thomas, *J. Polym. Sci. Polym. Symp.*, 1975, **49**, 203–210.
- 28 C. Crisafulli, R. Maggiore, S. Scirè and S. Galvagno, *J. Chem. Soc. Faraday Trans.*, 1994, **90**, 2809–2813.
- 29 S. Scirè, C. Crisafulli, R. Maggiore, S. Minicò and S. Galvagno, *Catal. Letters*, 1998, **51**, 41–45.
- 30 G. H. Yokomizo, C. Louis and A. T. Bell, *J. Catal.*, 1989, **120**, 1–14.
- 31 C. Crisafulli, R. Maggiore, S. Scirè and S. Galvagno, *J. Chem. Soc. Faraday Trans.*, 1994, **90**, 2809–2813.
- 32 K. Fujimoto, M. Kameyama and T. Kunugi, *J. Catal.*, 1980, **61**, 7–14.
- 33 M. M. T. Khan, G. Ramachandraiah and R. S. Shukla, *Polyhedron*, 1992, **11**, 3075–3081.
- 34 A. Sayari, J. Y. Shen and S. Kaliaguine, *Appl. Spectrosc.* 1992, **46**, 1279–1287.
- 35 Z. Luo, Z. Zheng, L. Li, Y.-T. Cui and C. Zhao, *ACS Catal.*, 2017, **7**, 8304–8313.
- 36 M. Niwa and N. Katada, *Chem. Rec.*, 2013, **13**, 432–455.



Scheme 1 Reaction pathway for conversion of pyroglutamic acid to 2-pyrrolidone. Broken arrows indicate side reactions.

Table 1 Ru particle size and amount of chemisorbed CO on Ru/MFI prepared using precursor solutions at various pH values.

pH	Ru particle size <sup>*1</sup> / nm	CO/Ru <sup>*2</sup>
1.8	3.0	0.05
2.8	3.3	0.05
3.7	5.8	0.02
6.0	9.2	0.03
8.9	8.0	0.03

<sup>\*1</sup> Ru average particle diameter in TEM images, <sup>\*2</sup> calculation based on CO chemisorption results.

Table 2 Ru particle size and amount of chemisorbed CO on Ru-loaded catalysts prepared using pH-adjusted  $\text{RuCl}_3$  solution.

Support	Ru particle size <sup>*1</sup> / nm	CO/Ru <sup>*2</sup>
$\text{SiO}_2$	8.3	< 0.01
$\text{Al}_2\text{O}_3$	3.2	0.14
FAU	2.8	0.03
MOR	5.1	0.02
*BEA	3.5	0.03
MFI	3.3	0.05

<sup>\*1</sup> Ru average particle diameter in TEM images, <sup>\*2</sup> calculation based on CO chemisorption results.

Table 3 Ru content, particle size, and amount of chemisorbed CO on Ru-loaded catalysts prepared by ion-exchange and impregnation.

	Support	Ru loading	Ru content / wt. %	Ru particle size <sup>*1</sup> / nm	CO/Ru <sup>*2</sup>
Ru/MFI-ie	MFI	Ion exchange	2.1 <sup>*3</sup>	2.8	0.04
Ru/MFI-imp	MFI	Impregnation	2.0 <sup>*4</sup>	3.2	0.03
Ru/Al <sub>2</sub> O <sub>3</sub> -imp	Al <sub>2</sub> O <sub>3</sub>	Impregnation	2.0 <sup>*4</sup>	3.1	0.06

<sup>\*1</sup> Ru average particle diameter in TEM images, <sup>\*2</sup> calculation based on CO chemisorption results, <sup>\*3</sup> calculation based on ICP results, <sup>\*4</sup> charged amount.

**Figure Captions**

- Figure 1 Screening of Ru-loaded catalyst supports for conversion of pyroglutamic acid. The catalysts were prepared in  $\text{RuCl}_3$  solution without pH adjustment.
- Figure 2 Influence of pH of precursor solution used for Ru/MFI preparation on product distribution in the conversion of pyroglutamic acid. The pH of the  $\text{RuCl}_3$  solution was adjusted by adding  $\text{NH}_4\text{OH}$  solution.
- Figure 3 IR spectra of adsorbed CO on Ru-loaded catalysts prepared in pH-adjusted  $\text{RuCl}_3$  solution.
- Figure 4 Product distributions in conversion of pyroglutamic acid on Ru-loaded catalysts prepared using pH-adjusted  $\text{RuCl}_3$  solution.
- Figure 5 IR spectra of adsorbed CO on Ru/MFI and  $\text{Ru}/\text{Al}_2\text{O}_3$  prepared by ion-exchange (ie) and impregnation (imp).
- Figure 6 Product distributions in conversion of pyroglutamic acid on (1) Ru/MFI-ie, (2) Ru/MFI-imp, and (3)  $\text{Ru}/\text{Al}_2\text{O}_3$ -imp. (1) was prepared by ion-exchange and (2) and (3) were prepared by impregnation.

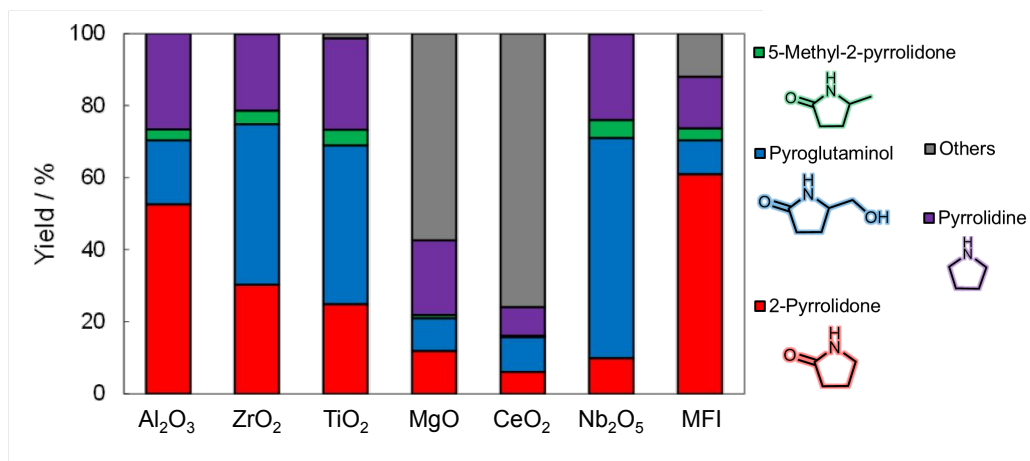


Figure 1

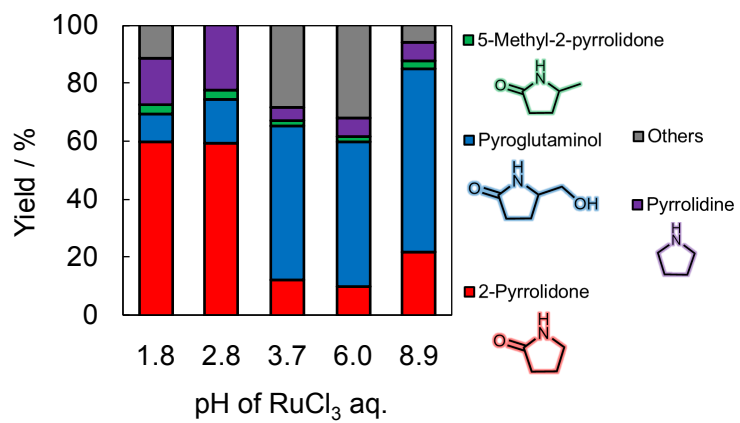


Figure 2

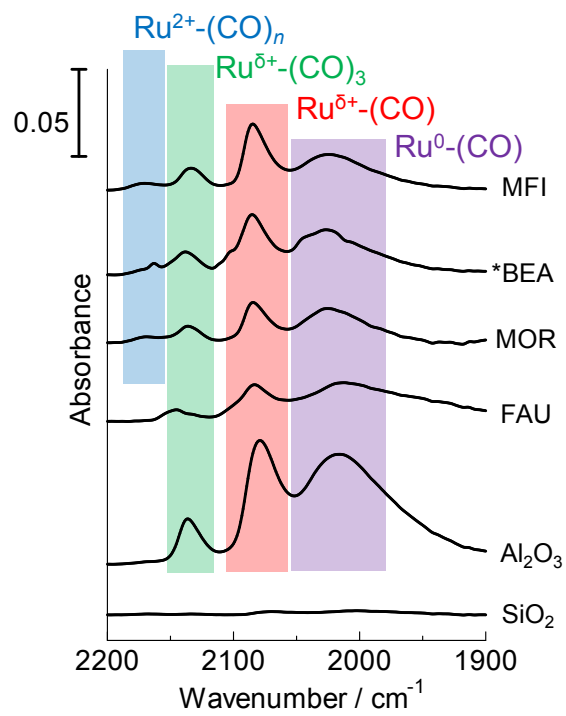


Figure 3

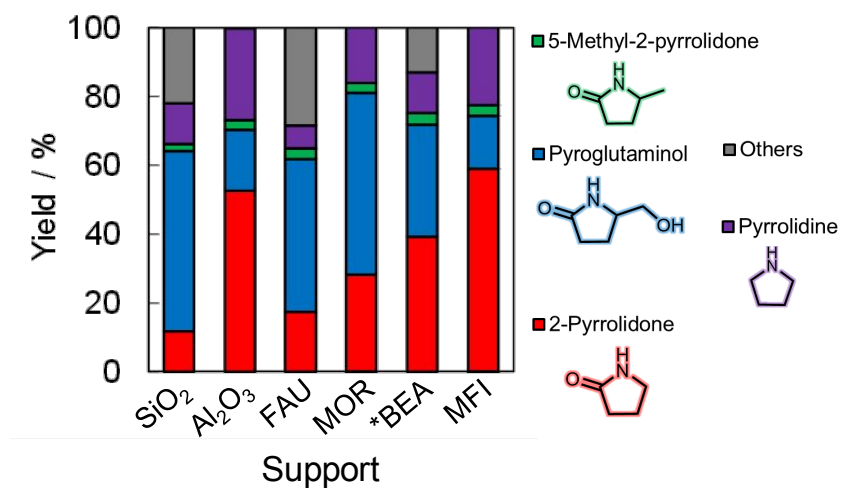


Figure 4

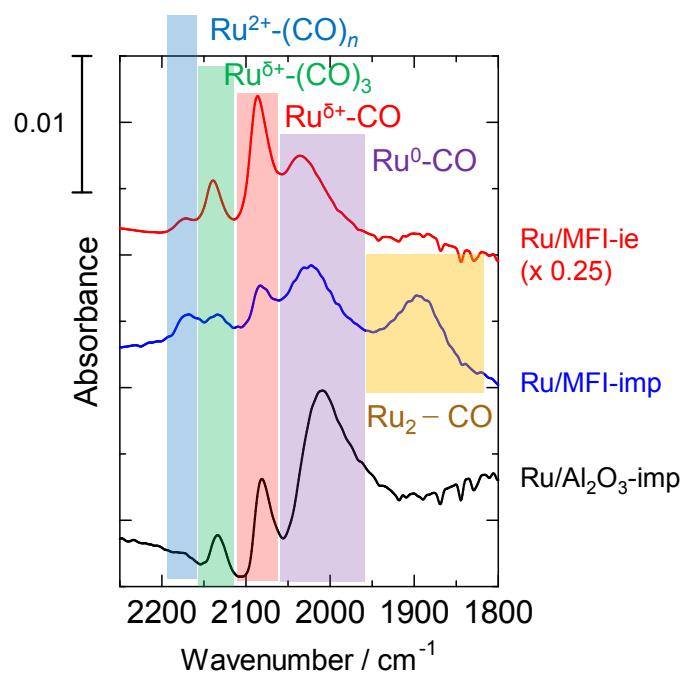


Figure 5

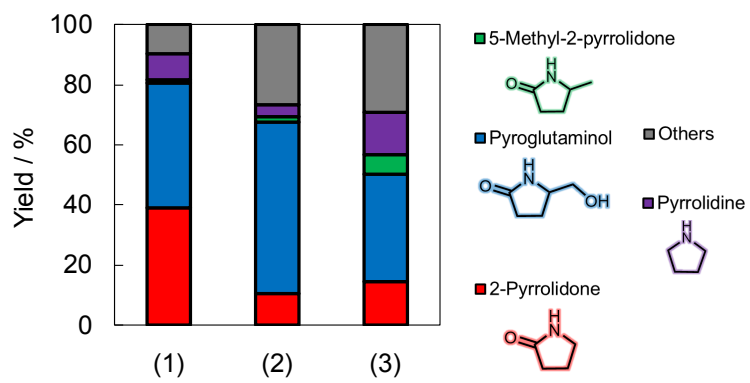


Figure 6